Structure, dynamics, and binding thermodynamics of the v-Src SH2 domain: Implications for drug design

ARTICLE *in* PROTEINS STRUCTURE FUNCTION AND BIOINFORMATICS · DECEMBER 2008

Impact Factor: 2.63 · DOI: 10.1002/prot.22119 · Source: PubMed

6 AUTHORS, INCLUDING:

Abdessamad Ababou
University of Cambridge
23 PUBLICATIONS **478** CITATIONS

SEE PROFILE

Rami Radwan
Anna University, Chennai
18 PUBLICATIONS **261** CITATIONS

SEE PROFILE

PROTEINS
STRUCTURE ■ FUNCTION ■ BIOINFORMATICS

Structure, dynamics, and binding thermodynamics of the v-Src SH2 domain: Implications for drug design

Jonathan D. Taylor,[1†] Abdessamad Ababou,[1†] Radwan R. Fawaz,[1] Christopher J. Hobbs,[2] Mark A. Williams,[1] and John E. Ladbury[1*]

[1] Department of Biochemistry and Molecular Biology, University College London, Gower Street, London, WC1E 6BT, UK
[2] Proximagen Neuroscience plc., Hodgkin Building, Guys Campus, Kings College London, SE1 1UL, UK

ABSTRACT

SH2 domains provide fundamental recognition sites in tyrosine kinase-mediated signaling pathways which, when aberrant, give rise to disease states such as cancer, diabetes, and immune deficiency. Designing specific inhibitors that target the SH2 domain-binding site, however, have presented a major challenge. Despite well over a decade of intensive research, clinically useful SH2 domain inhibitors have yet to become available. A better understanding of the structural, dynamic, and thermodynamic contributions to ligand binding of individual SH2 domains will provide some insight as to whether inhibitor development is possible. We report the first high resolution solution structure of the apo-v-Src SH2 domain. This is accompanied by the analysis of backbone dynamics and pK_a values within the apo- and peptide-bound states. Our results indicate that the phosphotyrosine (pY) pocket is tightly structured and hence not adaptable to exogenous ligands. On the other hand, the pocket which accommodates residues proximal and C-terminal of the pY (pY + 3) or so-called specificity determining region, is a large dynamic-binding surface. This appears to allow a high level of promiscuity in binding. Binding of a series of synthetic, phosphotyrosyl, peptidomimetic compounds designed to explore interactions in the pY + 3 pocket further demonstrates the ability of the SH2 domain to accommodate diverse ligands. The thermodynamic parameters of these interactions show dramatic enthalpy/entropy compensation. These data suggest that the v-Src SH2 domain does not have a highly specific secondary-binding site, which clearly presents a major hurdle to design selective inhibitors.

Proteins 2008; 73:929–940.

Key words: NMR spectroscopy; protein-ligand recognition; solution structure; thermodynamics; Src homology 2; specificity.

INTRODUCTION

Protein tyrosine kinases (PTKs) form an important contemporary class of pharmaceutical targets due to their role in many aspects of human cell behavior and proliferation. PTKs contain a kinase domain, responsible for phosphorylating specific tyrosyl residues, coupled to small accessory domains that modulate their activity, subcellular location, and enable formation of macromolecular signaling complexes. Thus, there are within a PTK several potential sites to use small molecules to inhibit its biological activity.

Many proteins, including PTKs, contain Src homology 2 (SH2) domains whose primary function is to bind to phosphotyrosyl (pY) residues presented by upstream receptors. The large number of SH2 domain-containing proteins which can potentially be expressed in a given cell, raises the important question of what is the level of specificity in these interactions.[1–4] This is broadly determined by variations in the recognition between the SH2 domain-binding surface and residues proximal to the target pY.[5–8] Most SH2 domains possess two distinct-binding pockets, one which binds the pY side chain and the other for the residue that is three positions C-terminal of the phosphotyrosine (pY + 3).[9] Other neighboring residues and sometimes water molecules make small but significant contributions to specificity in recognition.[10–12]

Additional Supporting Information may be found in the online version of this article.
Abbreviations: ARIA, ambiguous restraints for iterative assignment; BMRB, BioMagResBank; CNS, crystallography and NMR System; HSQC, heteronuclear single-quantum coherence; ITC, isothermal titration calorimetry; NMR, nuclear magnetic resonance; NOESY, nuclear Overhauser effect spectroscopy; PDB, protein data bank; pY, phosphotyrosine; SH2, Src homology 2.

Grant sponsors: BBSRC CASE studentship with UCB Celltech, an ORS award, and the Wellcome Trust.
[†]Jonathan D. Taylor and Abdessamad Ababou contributed equally to this work.
Jonathan D. Taylor's current address is Centre for Molecular Microbiology and Infection, Imperial College London, South Kensington, London, SW7 2AZ, United Kingdom.
Mark A. Williams's current address is School of Crystallography, Birkbeck, University of London, Malet Street, London, WC1E 7HX, United Kingdom.
*Correspondence to: John Ladbury, Department of Biochemistry and Molecular Biology, University College London, Gower Street, London, WC1E 6BT, United Kingdom.
E-mail: j.ladbury@biochem.ucl.ac.uk
Received 20 February 2008; Revised 10 April 2008; Accepted 17 April 2008
Published online 5 June 2008 in Wiley InterScience (www.interscience.wiley.com).
DOI: 10.1002/prot.22119

The observation that small polypeptides and peptidomimetics are able to compete for SH2-binding sites has encouraged the development of antagonists for this domain.[13–19] The two major drug design challenges are to replace the phosphotyrosine moiety with a stable, less negatively charged analog, and to increase the affinity/specificity of the inhibitor by exploring interactions in and around the pY + 3 pocket. Unfortunately, the pY pocket has remarkable preference for phosphotyrosine, whereas the pY + 3 pocket, usually preferring bulky aliphatic side chains, presents only a limited opportunity to develop specificity toward individual SH2 domains.[19,20]

The first reported PTK, *v*-Src, is a viral homologue of human c-Src (97% identical in sequence) and was discovered as the protein product of the Rous sarcoma virus oncogene, $p60^{v\text{-}src}$.[21,22] In mammalian cells, c-Src is a ubiquitously expressed nonreceptor protein tyrosine kinase.[23,24] The Src protein contains an SH2 domain that plays both a key role in autoregulation of kinase activity and in target protein recruitment.[2,25,26] The SH2 domain of this protein has been shown to interact with a number of proteins in tyrosine kinase-mediated signal transduction pathways (e.g., PDK1, focal adhesion kinase, and $p130^{cas}$) and is thus involved in several important cellular-signaling events.[27–29] For example, by binding to the PDGF receptor, it is able to inhibit stimulated cells from entering the S-phase of the cell cycle.[30] Hyperactive Src protein has been identified in a number of human malignancies,[31] including breast adenocarcinoma[32] and colon carcinoma.[33] Additionally, it has been shown to play a role in regulation of bone resorption in osteoclasts.[34–36]

Given the importance of the Src SH2 domain in cellular signaling, and as a drug target, a critical analysis of the structural, dynamic, and thermodynamic contributions to ligand recognition is likely to be important. Here, we present a solution structure of the *v*-Src SH2 domain in the absence of any ligand. In previously published structures, the Src SH2 domain is either found in complex with known ligands (i.e. tyrosylphosphopeptides or lead compounds), or the pY-binding site was occupied by an anionic buffer component.[9,37–41] Our investigation into the structure, dynamics and side-chain ionization states of *v*-Src SH2 provides additional insight into the nature of the binding interface. We find that the conserved glutamine, histidine, and arginine residues in the pY-pocket are held fixed by hydrogen bonds which results in a preformed pY-binding pocket, the structure, and dynamics of which are unchanged between the apo and peptide-bound forms. In contrast, the pY + 3-binding pocket is more dynamic in the apo-state and shows a significant reduction in conformational freedom upon ligand binding. Additionally, we measured the thermodynamic parameters for the binding of a series of peptidomimetic compounds, each of which contains a pY side chain but is coupled to a different chemical group in a position designed to explore the pY + 3 pocket.[42] Remarkably, all six of these diverse compounds bind to the Src SH2 domain with similar affinity as a result of extreme enthalpy–entropy compensation. The accommodation of these different chemical groups at the pY +3 site is apparently facilitated by the dynamic nature of the structure around the pY + 3 pocket.

METHODS

Sample preparation

The SH2 domain of *v*-Src (residues 144–249 of the full length kinase) was overexpressed in *E. coli* BL21 (DE3) pLysS using a pET3a plasmid kindly provided by Professor Gabriel Waksman. ^{15}N- and ^{13}C/^{15}N-labeled SH2 domain samples were produced by bacterial growth in M9 minimal medium supplemented with 1 g/L $^{15}NH_4Cl$ and 2 g/L unlabeled or $^{13}C_6$-labeled glucose as necessary. The SH2 domain was purified from the clarified cell supernatant by phosphotyrosine affinity chromatography and dialyzed into 20 m*M* MES (pH 6.0), 50 m*M* NaCl, and 1 m*M* DTT, which was used in all experiments except the pH titrations.

Structure determination

NMR data for structure determination were acquired using ~0.5 m*M* ^{15}N- or ^{13}C/^{15}N-labeled SH2 domain samples at 298 K on 500 and 600 MHz Varian UnityPlus or 800 MHz INOVA spectrometers. FID data were processed using NMRPipe, and resonance assignment was performed using ANSIG v.3.3.[43,44] Essentially, complete resonance assignments for the apo and peptide-bound forms of *v*-Src SH2 have been described previously.[45] NOESY assignment was performed in an automated manner using ARIA version 2.2, which interfaces to the CNS structure calculation software.[46,47] A list of 4443 unassigned NOEs derived from two ^{15}N-edited NOESY-HSQC spectra (mixing times 50 and 200 ms) and two ^{13}C-edited NOESY-HSQC spectra (the aliphatic and aromatic regions were recorded separately) were used as an input for ARIA. During the final iteration 1473 redundant restraints were discarded. The ND1 atoms of H58 and H96 were treated as deprotonated in order to reflect the actual ionization state of these residues revealed by our pK_a measurements. Backbone–backbone hydrogen bonds were identified in converged structures from intermediate iterations, and 41 hydrogen bond restraints were included in the final iteration. From the 200 structures generated by simulated annealing the 120 lowest-energy structures were refined in a shell of explicit water by ARIA/CNS according to the default protocol. A group of 20 structures, displaying the best stereochemistry and lowest restraint violation energetic penalty, were selected to be a representative ensemble and deposited in the PDB under accession code 2JYQ.

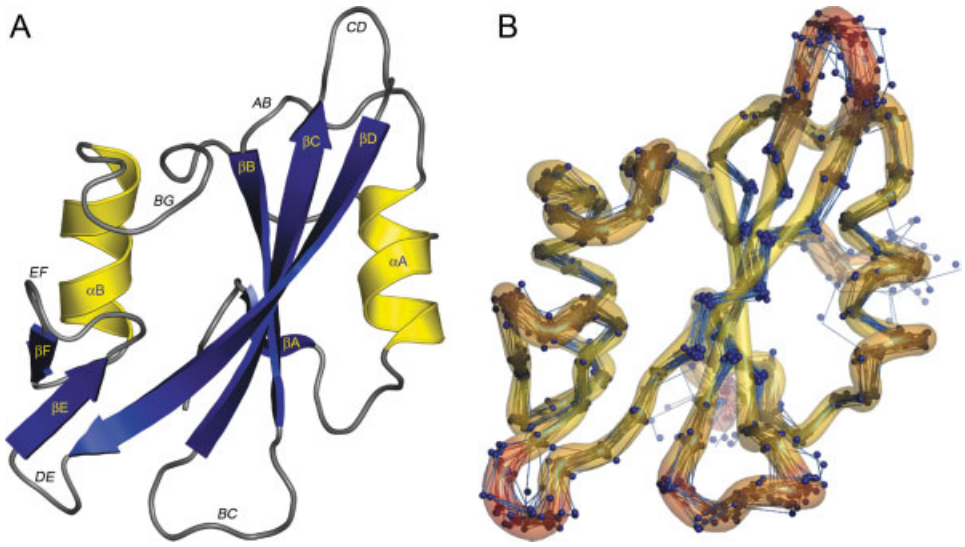

Figure 1

Solution structure of v-Src SH2. **A:** Cartoon representation of the mean structure, with secondary structure labeled according to the nomenclature in Waksman et al.[39] Loop regions are shown in italics. **B:** Worm representation of the ensemble. The average RMSD of CA atoms (blue spheres) from mean CA atomic coordinates was used to color the worm surface in a yellow → red gradient. This figure was generated using PyMOL.[51]

Relaxation analysis

^{15}N-edited R_1, R_2, and {^{1}H}-^{15}N NOE experiments, recorded at 800 MHz, were used to measure the mobility of backbone amides in *v*-Src SH2 in the apo and peptide-bound states. Relaxation delays used in the R_1 experiment were 10.1, 40.2, 80.5, 161, 322, 644, 966, 1288, and 1610 ms. Delays in the R_2 experiment were 33.2, 66.4, 99.6, 133, 166, 199, 233, 266, 299, and 332 ms. Cross-relaxation NOE data were recorded corresponding to the saturated and nonsaturated state. Peak heights were calculated in ANSIG,[44] and errors were estimated directly from the variation between experiments with replicated relaxation delays. R_1 and R_2 values were obtained by nonlinear least-squares fitting of the changes in peak intensity with relaxation delay to a single exponential decay function. The fitted relaxation rates and calculated NOE ratios were then used to estimate the overall tumbling time (τ_m) of the SH2 domain. Amides that displayed large amplitude fast motions or slow chemical exchange processes were excluded from this calculation. Relaxation data for each amide were finally fitted to models of bond vector motion described by the Lipari-Szabo formalism.[48,49] All relaxation calculations were performed using in-house Mathematica (Wolfram Research, Champaign, USA) scripts.

pH titration

pK_a values for selected ionisable groups within the apo and peptide-bound SH2 domain were obtained from HSQC spectra recorded across the pH range 5.0–9.0 in steps of 0.5 pH units. To minimize changes in ionic strength during the titration, the SH2 domain was dialyzed into a triple-buffer system containing 25 m*M* sodium acetate, 25 m*M* MES, 50 m*M* TRIS, 50 m*M* NaCl, and 1 m*M* DTT. NH and CH resonances were monitored via ^{1}H-^{15}N HSQC and constant time ^{1}H-^{13}C HSQC spectra. The pK_a of the phosphate within the phosphopeptide was obtained via ^{31}P NMR spectroscopy. Chemical shift changes were fitted to the modified Henderson-Hasselbalch equation[50]:

$$\delta = \left[\delta_{acid} + \delta_{base} 10^{(pH-pK_a)}\right] \Big/ \left[1 + 10^{(pH-pK_a)}\right] \qquad (1)$$

where δ is the chemical shift of the observed resonance at a given pH and δ_{acid} and δ_{base} are the chemical shifts corresponding to protonated and deprotonated species, respectively.

Isothermal titration calorimetry

ITC was used to investigate the thermodynamics of binding for the peptide Ac-PQpYEEIPI-NH_2 and a group of six closely related synthetic compounds. All experiments were performed at 25°C using a VP-ITC microcalorimeter (MicroCal, Northampton, MA) by serial injection of 500 μ*M* ligand into a sample containing 50 μ*M* *v*-Src SH2 domain, with a re-equilibration period of 3.5 min separating each of the ~20 injections. In each case, the heat of dilution was determined separately by

Table I
A Statistical Summary of the *v*-Src SH2 Structure Calculations

Restraint type (number)		Mean ± σ
Unambiguous restraints (2067)	RMSD (Å)	0.007 ± 0.001
	No. of violations > 0.3 Å	0.02 ± 0.14
	No. of violations > 0.1 Å	1.68 ± 1.24
Ambiguous restraints (862)	RMSD (Å)	0.005 ± 0.001
	No. of violations > 0.3 Å	0 ± 0
	No. of violations > 0.1 Å	0.3 ± 0.45
Hydrogen bond restraints (41)	RMSD (Å)	0.013 ± 0.004
	No. of violations > 0.3 Å	0 ± 0
	No. of violations > 0.1 Å	0.06 ± 0.24
Structural quality index		**Value ± σ**
Global atom RMSD (Å)	Backbone atoms	0.90 ± 0.16
	Heavy atoms	1.62 ± 0.23
Average RMSD from mean structure (Å)	2° structure, backbone atoms	0.39 ± 0.14
	All backbone atoms	0.64 ± 0.09
	All heavy atoms	1.16 ± 0.10
Deviations from ideal geometry	Bond lengths (Å)	$3.7 \times 10^{-3} \pm 0.1 \times 10^{-3}$
	Bond angles(°)	0.51 ± 0.02
	Impropers (°)	1.46 ± 0.11
Ramachandran plot analysis	Most favored (%)	81.2 ± 1.9
	Additionally allowed (%)	16.8 ± 1.8
	Generously allowed (%)	0.7 ± 0.8
	Disallowed (%)	1.3 ± 0.4
CNS energies (kcal/mol)	E_{total}	−3842.5 ± 101.1
	E_{bonds}	22.6 ± 1.8
	E_{angles}	110.8 ± 7.7
	$E_{impropers}$	65.2 ± 9.7
	$E_{dihedrals}$	516.3 ± 6.5
	E_{vdw}	−504.2 ± 17.0
	$E_{electrostatics}$	−4081.2 ± 97.9
	E_{noe}	27.9 ± 13.6

the titration of the ligand into buffer alone. Data were fitted to a single site-binding model using ORIGIN (MicroCal, Northampton, MA). The fitted binding stoichiometry was between 0.8 and 1.3 for all experiments.

RESULTS AND DISCUSSION

Solution structure of v-Src SH2

The solution structure ensemble of the apo form of the *v*-Src SH2 domain has the familiar overall fold of a central β-sheet flanked by two α-helices [Fig. 1(A,B)], which is shared by almost all members of the SH2 family. A statistical summary of the experimental restraints and quality indices regarding the ensemble is provided in Table I. The secondary structural regions of *v*-Src SH2 are particularly well defined with a mean backbone root mean square deviation (RMSD) from the average structure of 0.39 ± 0.14 Å.

A comparison of the apo *v*-Src SH2 structural ensemble with the phosphate-bound crystal structure of the same domain (PDB code 1SPR[39]) revealed a high degree of overall similarity (see Fig. 2 for a structural alignment). The mean RMSD between the crystal structure and individual NMR conformers for residues 4–102 is 1.5 ± 0.2 Å for backbone atoms and 2.2 ± 0.2 Å for heavy atoms. The most notable difference between the NMR ensemble and the previously published crystal structure is the position of the EF and BG loops, which form the pY + 3-binding site. In the former case, these loops are considerably closer together than in the crystalline form (5.5 Å vs. 9.2 Å separating CA atoms of T72 and G93). Consequently, the pY + 3-binding pocket is shallower and less clearly defined in the NMR ensemble. It is not obvious whether this difference is related to the conditions used for each structure determination or to the presence of phosphate in the crystal structure. Whilst overall differences are small, the structure presented here should be considered as a more realistic apo form of *v*-Src SH2 compared to the existing "peptide-free," yet phosphate-bound, crystal structure. This structure will complement continuing biophysical and molecular dynamics studies and potentially provide a new target for small molecule-docking calculations.

Phosphotyrosine-binding site

The pY pocket of the SH2-binding site is highly specific for phosphotyrosine.[53] This is necessary to ensure

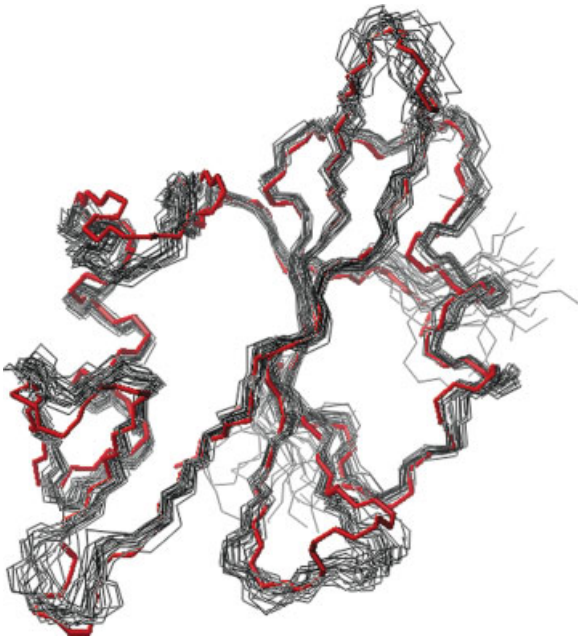

Figure 2
Comparison of the NMR ensemble with the peptide-free crystal structure. Backbone heavy atoms from residues 4–102 were used to superimpose the NMR ensemble (black lines) onto the peptide-free crystal structure (red sticks) of *v*-Src SH2. The RMSD between the mean NMR structure and the crystal structure is 1.3 Å. This figure was generated using MOLMOL.[52]

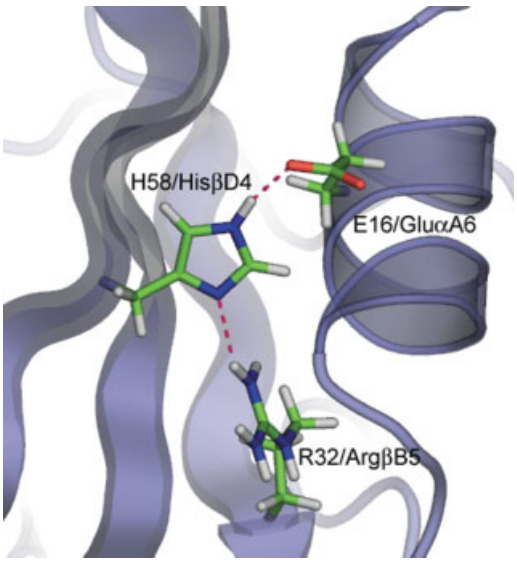

Figure 3

Hydrogen bonding triad within the pY-binding site. A network of hydrogen bonds within the apo *v*-Src SH2 domain structure serves to restrain the ArgβB5 side chain such that it is poised to interact with the phosphate group of pY. This figure was generated using PyMOL.[51]

that the domain does not interact with other posttranslationally phosphorylated species or unmodified tyrosine present in the cellular environment.[54] The original structure of the phosphopeptide-bound SH2 domain (1SPS) revealed that this selectivity is afforded by a deep polar pocket, which is fully dehydrated when occupied by phosphotyrosine and the SH2 domain sidechains make 15 hydrogen bonds to the phosphotyrosine (including to the aromatic ring). Thermodynamic study has shown that this interaction is entropically driven at 25°C. The hydrogen bonds to phosphotyrosine apparently compensate enthalpically for those which were made to water in the apo-state, and the entropy associated with solvent release is thought to dominate binding.[19]

We note a few potential reasons why the selectivity of the pY pocket is so strong. First, all but one of the residues that interact with pY are located within regions of secondary structure, causing their geometric arrangement to be preserved. The exception is T36, which is located at the N-terminal end of the BC loop. Second, several of the residues lining the pocket have short side chains (S34, T36, and C42), which reduces the number of degrees of freedom in the binding site. Third, a network of hydrogen bonds is apparent within the pY-binding site connecting a triad of conserved side chains: E16/GluαA6, H58/HisβD4, and R32/ArgβB5 (see Fig. 3). The conformation of the guanidino group of R32, which forms the most important contact to the phosphotyrosine, is restrained by partial burial and formation of a stable hydrogen bond with H58. R32 is absolutely conserved within the FLVRES sequence found in all SH2 domains and mutation of this residue renders the pocket incapable of recognizing pY.[53] Thus, there appears to be rather little adaptive potential in the pY-binding site toward non-phosphotyrosyl ligands.

Chemical shift perturbations induced by peptide binding

The response of *v*-Src SH2 amide chemical shifts toward peptide binding allowed us to characterize both the site of interaction and detect overall alteration in domain structure. The combined chemical shift changes observed for backbone amides are shown in Figure 4. The largest perturbation is shown by E35, which forms a direct hydrogen bond with the phosphate group, and is strongly affected by the ring-current electromagnetic field of pY. Other large perturbations are observed for amides in and around the peptide-binding site, particularly in the EF and BG loops that are directly involved in binding the pY + 3 side chain. The absence of significant chemical shift changes occurring on the opposite side of the domain to the binding site, or in distal loops suggests that peptide binding does not induce any gross changes in the domain structure. This is consistent with the lack of gross structural changes previously observed in the peptide-free and peptide bound crystal structures (1SPR vs. 1SPS). It is interesting to note that the backbone amide of R32 shows only a very minor change in chemical shift, whereas the side chain amide of this residue displays a significant combined $^{1}H/^{15}N$ perturbation of 0.77 that is consistent with the binding of pY.

Backbone dynamics of v-Src SH2

The dynamic behavior of backbone amides within apo- and PQpYEEIPI-bound *v*-Src SH2 was investigated using NMR-relaxation experiments. Empirical longitudinal (R_1) and transverse relaxation (R_2) rates were used to determine the overall rotational correlation times (τ_c) for the apo-domain (6.21 ± 0.10 ns) and SH2-peptide complex (6.74 ± 0.15 ns). These results are slightly smaller than those obtained for another Src-family SH2 domain (Hck) where the peptide-free and peptide-bound values were 6.8 ns and 7.6 ns, respectively.[55] The Lipari-Szabo approach was used to generate S^2 (order parameter) data for each backbone amide.[48,49] The changes in S^2 values observed for the *v*-Src SH2 domain on binding peptide are shown in Figure 5 (also see Supplementary Figs. 1 and 2 for full results of relaxation analysis). There are two notable patterns within these results. First, the amides of residues contributing to the pY-binding site do not appear to undergo significant change in order parameter on peptide binding, except for the BC loop, which becomes slightly more ordered in the presence of

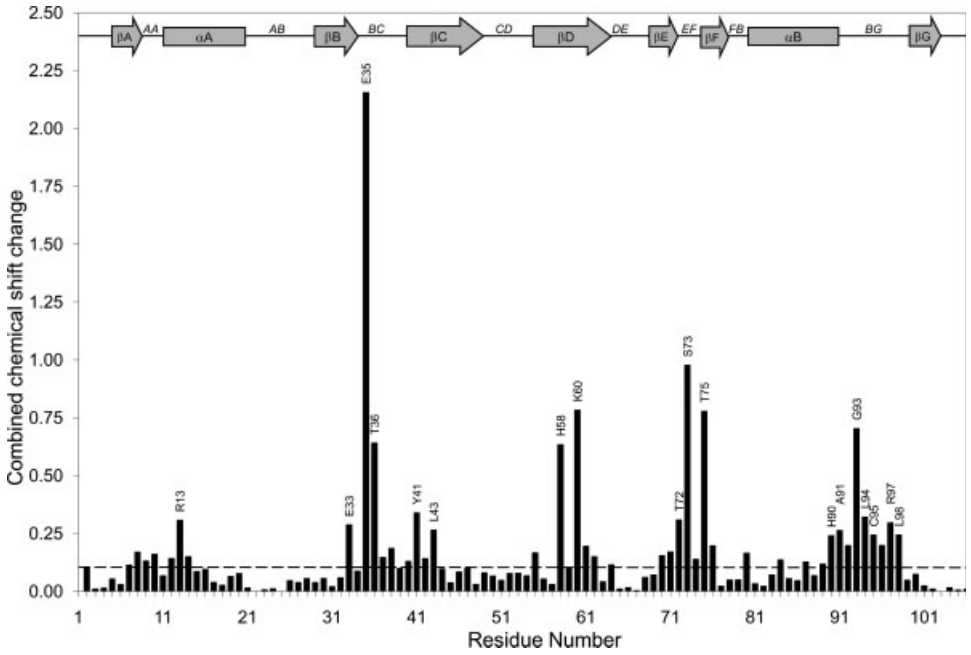

Figure 4

Chemical shift changes displayed by backbone amides within *v*-Src SH2 induced by binding of PQpYEEIPI. The combined chemical shift change is calculated as follows: $(\Delta\delta_{tot}) = \Delta\delta^{1}H + \Delta\delta^{15}N/6.4$. A threshold shift change of 0.1 identifies residues that undergo significant change whilst those displaying values above 0.2 are labeled. The *v*-Src SH2 secondary structure is displayed at the top of the figure, with β-strands and α-helices indicated by arrows and rectangles, respectively.

peptide. Thus, these dynamics data appear to confirm the proposition that the pY pocket is largely predefined before binding. Second, amides within the pY + 3-binding site tend to show an increase in backbone rigidity on binding peptide consistent with a general restriction of loop motion. It is also noticeable that binding of the peptide within this region has a more widespread effect on local dynamics than the interaction between the pY side chain and its cognate pocket. The dynamic behavior of the EF and BG loops, which control the size and shape of the pY + 3 pocket in the apo-state, are expected to contribute toward the observed ability of the pY + 3

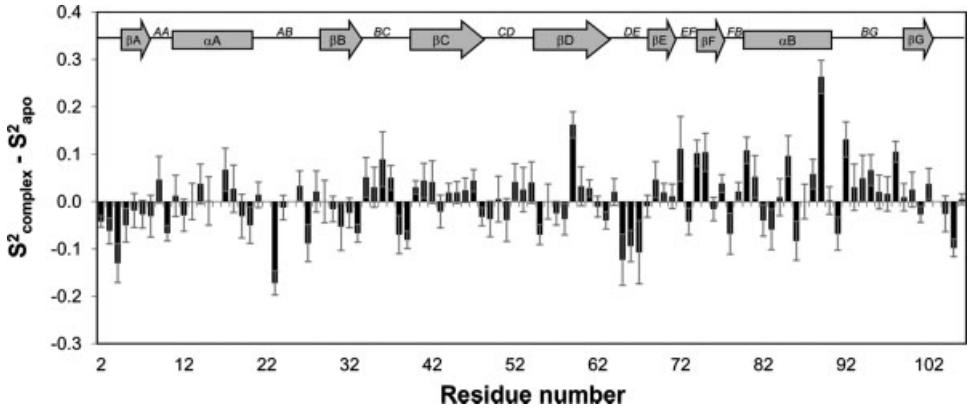

Figure 5

Difference in S^2 values for backbone amides in *v*-Src SH2 ($S^2_{complex}$ minus S^2_{apo}). The error bars reflect the combined error in calculation for both data sets according to the formula: combined error = $\mathrm{sqrt}[(\delta S^2_{complex})^2 + (\delta S^2_{apo})^2]$. The figure is annotated with secondary structural information, with β-strands and α-helices indicated by arrows and rectangles, respectively.

Table II
Thermodynamic Data Obtained from an ITC Analysis of the PQpYEEIPI Peptide and Compounds 1–6

SH2 ligand	K_B ($\times 10^6$ M^{-1})	ΔH_b (kJ/mol)	$T\Delta S$ (kJ/mol)	ΔG^o_b (kJ/mol)
PQpYEEIPI	10.0 ± 0.06	−34.8 ± 0.15	5.1	−39.9
1	1.07 ± 0.06	−27.2 ± 0.16	7.2	−34.4
2	2.09 ± 0.63	−23.3 ± 0.64	12.8	−36.1
3	1.96 ± 0.49	−18.2 ± 0.43	17.8	−36.0
4	5.79 ± 0.19	−20.8 ± 0.33	17.8	−38.6
5	1.93 ± 0.17	−18.2 ± 0.15	17.7	−35.9
6	1.41 ± 0.26	−16.8 ± 0.32	18.3	−35.1

pocket to accept a range of diverse chemical groups within biologically relevant or synthetic SH2 ligands.[56,57] In the unliganded state, the EF and BG loops are relatively disordered. However, on binding of the specific peptide, the S^2 values of backbone amides within these loop residues increase are consistent with a general restriction of loop motion. A relatively rigid pY + 3 pocket in the presence of peptide ligand has also been observed in the studies of SH2 domains of SAP and the p85α subunit of PI3K, Syp, and Hck.[55,57–59]

pK_a of side chains within the pY pocket

The interaction in the pY-binding site of *v*-Src SH2 was explored further by monitoring the ^{1}H chemical shifts of backbone and side chain resonances as a function of pH. Because local electron distributions and hence chemical shifts are strongly affected by protonation events, these data yield apparent pK_a values for ionisable side chains as reported by the change in chemical shift of neighboring nuclei. The phosphate pK_a of the peptide ligand in the free and bound states was similarly measured using the ^{31}P chemical shift. Results for selected residues are described below; the full data set is provided in Supplementary Tables I and II.

The *v*-Src SH2 domain contains three histidine residues; H90 and H96 in the BG loop and H58 in the pY pocket. NMR chemical shift data show that H90 and H96 Hε1 protons, which are proximal to the ionisable Nδ1 atom, have strong pH-dependent chemical shift profiles, yielding apparent pK_a values of 6.4 and 5.7, respectively [Fig. 6(A,B)]. Such values are close to the typical pK_a of solvent-exposed histidine residues (6.2–6.3) and to that of free histidine (6.0). In contrast, the H58 Hε1 resonance is pH-insensitive across the range measured indicating a pK_a value below 4.0 in both the apo and peptide-bound states. These data show that H58 is essentially uncharged at physiological pH in both the apo and peptide-bound forms of *v*-Src SH2. The origin of this effect can be explained on two levels by considering the interaction of H58 with R32 (see Fig. 3). First, the positive electrostatic field that surrounds the guanidinium moiety of R32 would be expected to destabilize the positively charged form of H58, thus lowering its pK_a. Second, a hydrogen bond appears to exist between the $N_{\delta 1}$ position on H58 and the NH_η position on R32. This interaction is clearly evident within the ensemble of solution structures described in this study and would account for the substantial lowering of the H58 pK_a value. Also predicted within the ensemble is a hydrogen bond between the $NH_{\varepsilon 2}$ of H58 and a carboxylate oxygen of E16/GluαA6, which completes a structural triad at the base of the pocket (see Fig. 3). Thus, the side chain of H58 makes important bridging interactions between E16 and R32 that probably serves to maintain a particular orientation of the latter. The E16/H58 interaction is also observed within the peptide-bound X-ray crystallographic structure of *v*-Src SH2 (PDB code 1SPS); however, the R32/H58 hydrogen bond is not observed due to refinement of the structure using the fully protonated form of histidine. On the basis of the observed pK_a values, we

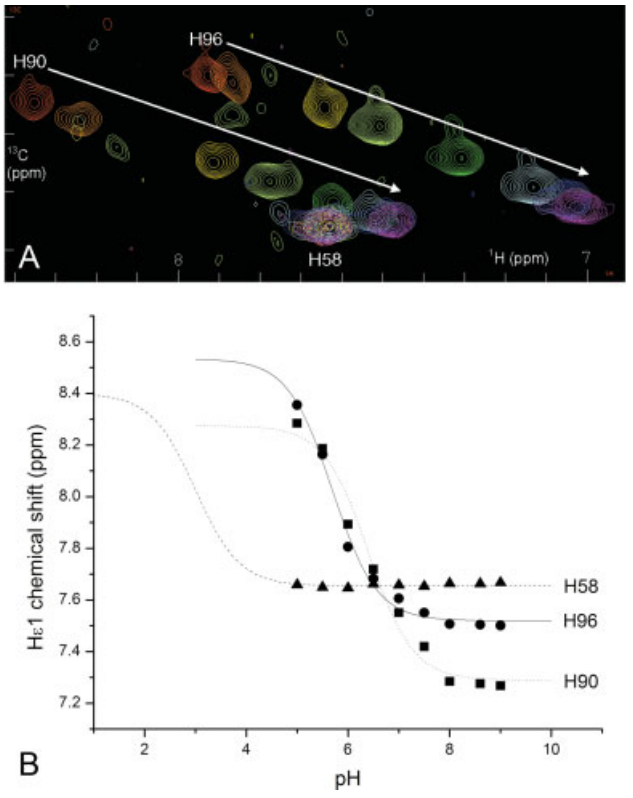

Figure 6
Measurement of the apparent pK_a of histidines within *v*-Src SH2. **A:** The histidine CH_ε region of the $^1H^{13}C$-HSQC spectrum of peptide-bound *v*-Src SH2 recorded at pH values between 5.0 (red contours) and 9.0 (magenta contours). The resonances of H90 and H96 are pH dependent, as indicated by the white arrows, however that of H58 did not move during the titration. **B:** Histidine $H_{\varepsilon 1}$ chemical shifts (H58 triangles, H90 squares, and H96 circles) of peptide-bound *v*-Src SH2 as a function of pH, with best-fit lines generated by ORIGIN. A simulated titration curve is displayed for H58.

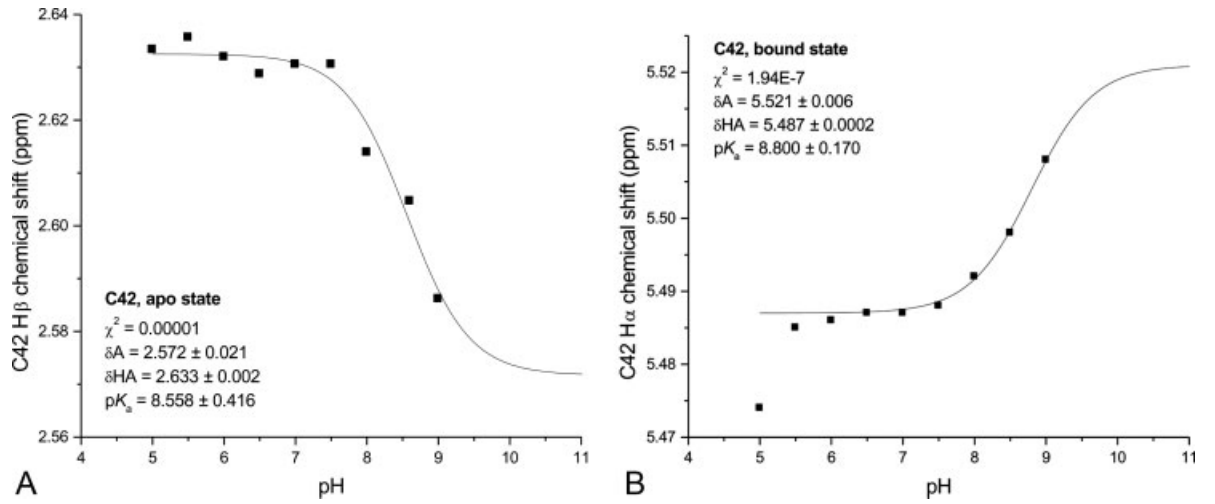

Figure 7

Measurement of the apparent pK_a of C42 (CysβC3). **A:** Mathematical fitting of C42 Hβ chemical shift as a function of pH (apo domain), results shown inset. **B:** C42 Hα chemical shift as a function of pH (peptide-bound complex). The change in chemical shift between pH 5 and 6 is attributed to ionization of the neighboring phosphate (pK_a 4.9) within the complex.

fully expect these hydrogen bonds to exist in both the apo- and peptide-bound states.

It is not clear how widely observed the hydrogen-bonded triad arrangement of amino acids is in influencing the interactions of the Src family or other SH2 domains. On one hand, the interaction between R32 (ArgβB5) and H58 (HisβD4) seems important because these residues are highly conserved throughout the SH2-domain family.[7,60] A manual inspection of the structures of SH2 domains available in the PDB indicated that the hydrogen bond connecting HisβD4 and ArgβB5 is not always present. However, some structures were refined using the fully protonated form of histidine, which would preclude formation of this hydrogen bond. To date, the HisβD4/ArgβB5 hydrogen bond has only been explicitly reported for the C-terminal SH2 domain of PLCγ_1.[60] In this system, HisβD4 also displayed a pK_a value below 4 in the apo and peptide-bound states, and the chemical shifts of the side chain nitrogens were consistent with deprotonation at the $N_{\delta 1}$ position.[60] On the other hand, *in vitro*-binding studies suggest that the presence of this hydrogen bond is not essential to binding because mutation of H58 to alanine resulted in only a twofold decrease in affinity compared to wild type.[53]

C42/CysβC3 plays a prominent role in the pY-binding pocket. It has been suggested that ionization of this thiol may be responsible for the suboptimal peptide-binding affinities observed above pH 7.5.[61] Determination of chemical shift changes over a range of pH revealed that C42 displays pK_a values of 8.56 ± 0.42 and 8.80 ± 0.17 in the apo and bound states, respectively [see Fig. 7(A,B)]. These measurements for C42 agree with pK_a values derived from the pH dependence of binding affinity determined by ITC experiments (8.2 ± 0.7 and 8.5 ± 0.7 for the apo and peptide-bound forms, respectively).[61] The herein data thus confirm the speculation of the authors of the ITC study that the changes in binding affinity in this pH range are due to the protonation state of C42. Furthermore, the pK_a values in the free and bound states are sufficiently similar as to suggest that there is only a small effect on the net electrostatic environment surrounding the thiol as a result of pY binding at physiological pH and that there is no direct interaction with the phosphate. This is consistent with the crystal structure of the complex in which the SH group is 5Å from the phosphate. Thus, our results support the view that deprotonation of C42 is slightly detrimental to the binding of phosphopeptides due to electrostatic repulsion.

In addition, the Cys42 side chain has been associated with a weak phosphoesterase activity that may serve to regulate the binding affinity or timescale of interaction between phosphopeptides and the Src SH2 domain.[62] The increased preference for the thiol to be deprotonated in the context of the pY-binding site, manifested in the ~0.5–0.8 pH unit decrease in pK_a compared to solvent-exposed cysteine (pK_a ~ 9.3), might explain the reported increased catalytic activity of this thiol at physiological pH. The reactivity of this cysteine has been exploited on occasion in the design of Src SH2-specific inhibitors.[15,63,65]

The pK_a value of the secondary phosphate ionisation ($PO_4^- \leftrightarrow PO_4^{-2}$) from the peptide used in these studies was also determined using ^{31}P NMR spectroscopy

[Fig. 8(A)]. The free peptide yielded a pK_a value of 6.22 ± 0.02 [see Fig. 8(B)], which is essentially identical to previous measurements of this and other phosphotyrosyl peptides.[13,60,61] Upon binding to *v*-Src SH2, the phosphate pK_a decreased to 4.90 ± 0.18 [see Fig. 8(C)], which is in fairly close agreement with the results from the pH dependence of peptide affinity (4.4 ± 0.3).[61] This substantial change in pK_a indicates that the PO_4^{2-} form of pY is strongly favored in the bound state.

Thermodynamic analysis of ligands

ITC was used to characterize the binding thermodynamics of a small group of synthetic SH2 domain ligands [1–6 in Fig. 9(A)] and of the biological target peptide, PQpYEEIPI. Compounds 1–6 were designed to explore interactions in the pY + 3 pocket and are peptidomimetics based upon a bicyclic aminopyrridazionodiazepine scaffold, which replaces the central Glu-Glu region of the peptide that is attached to a phosphotyrosyl side chain.[42] The ligands differ only with respect to the side chain that was designed to insert into the pY + 3 pocket. This range of compounds is therefore suited to investigate the contribution of the pY + 3 pocket to the binding specificity of the *v*-Src SH2 domain. The results for the binding thermodynamics of each compound are given in Table II [typical ITC data are shown in Fig. 9(B)]. In each case, the synthetic ligands displayed binding affinities are between 2- and 10-fold weaker than the natural peptide. The favorable increases in $T\Delta S$ observed for 1–6 compared to the peptide may reflect the release of water molecules from the complex. In the X-ray crystal structure of the Src SH2 domain bound to the pYEEI-based peptide ligand, a network of water molecules is observed on the complex interface, which is sustained through hydrogen bonding with the side chain of the Glu residue in the pY + 2 position.[39] The synthetic compounds, in removing this side chain, preclude interaction with these water molecules. The consistently smaller favorable contribution to the enthalpy of binding and greater favorable $T\Delta S$ observed for 1–6 compared to the peptide may, respectively, reflect the loss of water-mediated interactions between ligand and protein and the consequent additional release of water molecules upon complex formation. A possible further contribution to the favorable $T\Delta S$ in the interactions of compounds 1–6 may be the inherently lower flexibility of the bicyclic scaffold and hence reduction in restriction in conformational freedom on complex formation.

It is remarkable that despite the differences in the chemical moiety designed to probe the pY + 3-binding pocket, the affinities of the interactions of the six compounds analyzed are highly similar (i.e. all within an order of magnitude). This suggests a highly promiscuous binding site which can accommodate these different chemical groups. Although the binding of 1–6 to *v*-Src

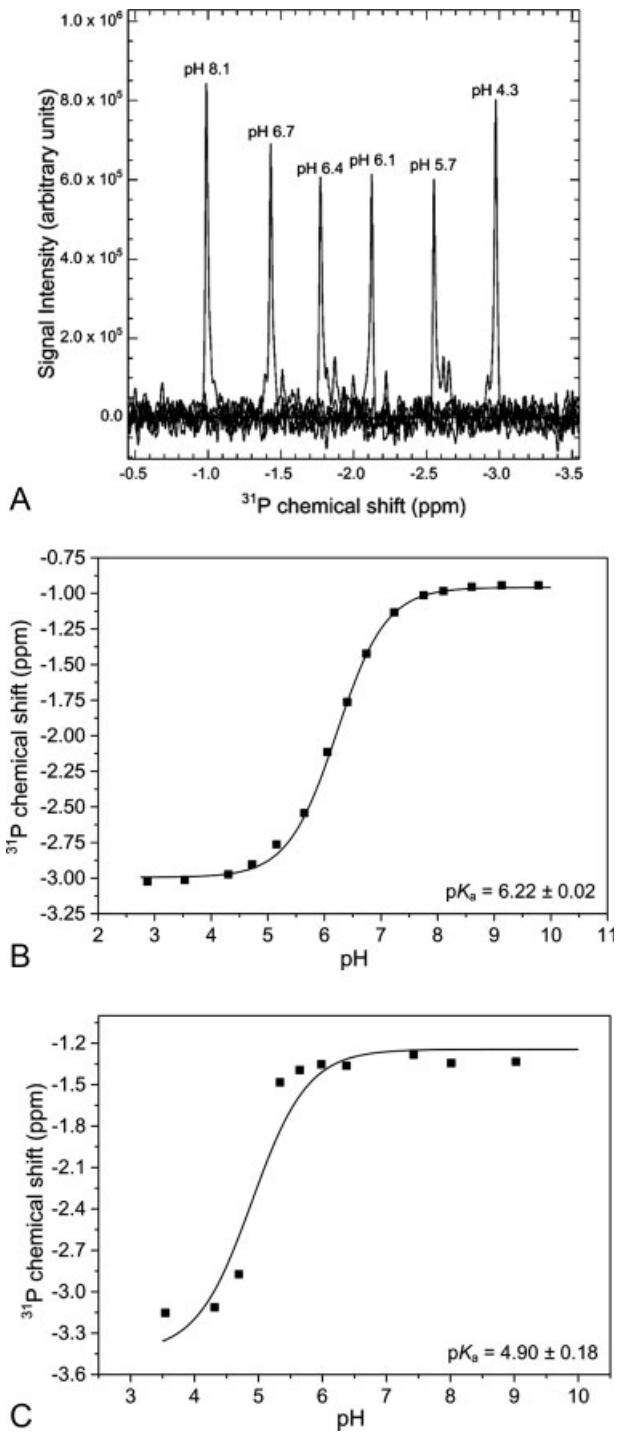

Figure 8

Measurement of the phosphate pK_a within PQpYEEIPI. **A:** Overlaid 31P-NMR 1D spectra of free phosphopeptide recorded at selected pH values as labeled. **B** and **C:** Mathematical fitting of the observed changes in ^{31}P chemical shift with pH for the free and *v*-Src SH2-bound phosphopeptide forms, respectively, with resultant pK_a values shown inset.

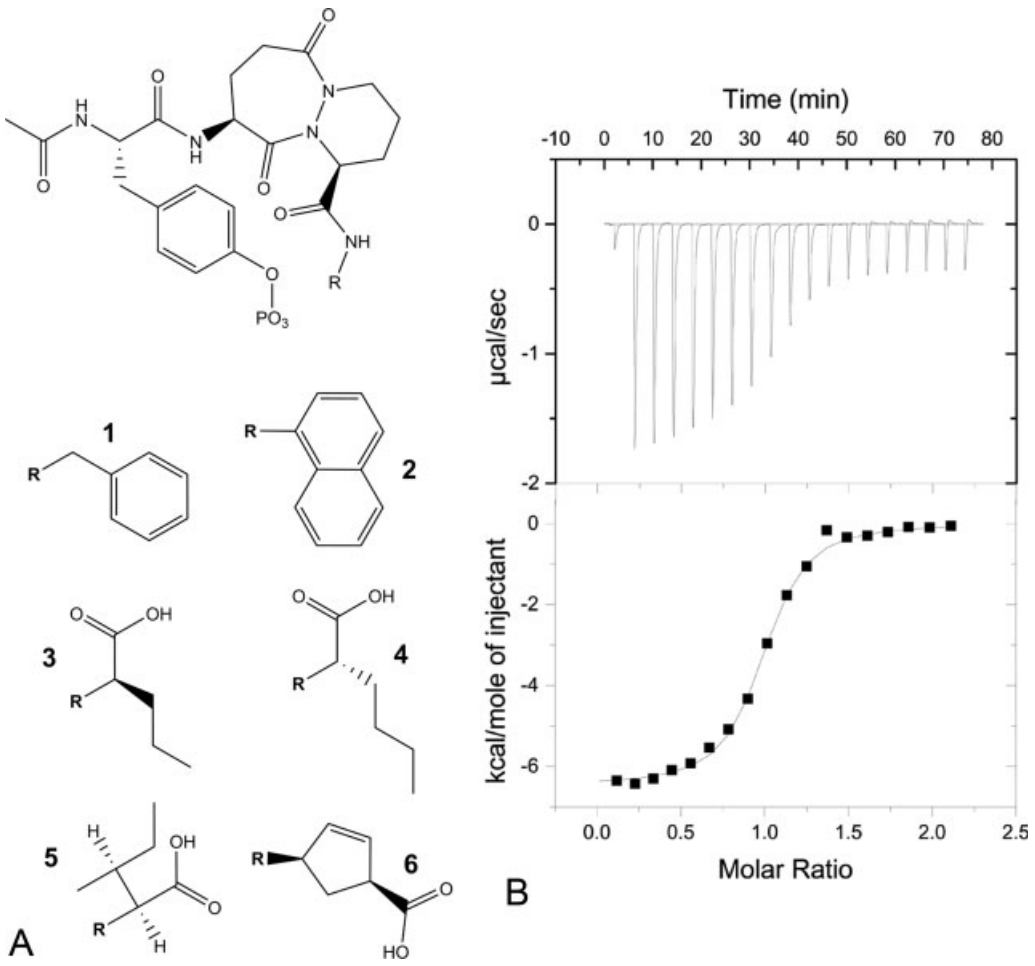

Figure 9

Structures of peptidomimetic compounds and ITC (**A**) chemical structures of compounds 1–6. **B:** Exemplary binding isotherm for compound 1. Full thermodynamic results are shown in Table II.

SH2 display similar overall free energy changes, the enthalpy, and entropy contributions to binding differ significantly. The ITC and NMR data suggest that the dynamic flexibility of the pY + 3 pocket results in a compensatory effect of the ΔH and $T\Delta S$. For example, compound 1 displays a large change in enthalpy ($\Delta H = -27.2$ kJ/mol) yet a relatively small change in entropy ($T\Delta S = 7.2$ kJ/mol). Whereas for compound 6, the $T\Delta S$ is more favorable (18.3 kJ/mol), however this is compensated for by a less favorable enthalpy change on binding (−16.8 kJ/mol). The net effect is that these synthetic side chains may be accommodated by the SH2 domain with little or no change in binding free energy (ΔG) and hence affinity.

CONCLUSIONS

This work further emphasizes the inherent difficulties in targeting SH2 domains with small molecular inhibitors. In this example, the strong specificity of the pY pocket is based upon a well-defined binding pocket rigidified by secondary/tertiary structure and a small hydrogen-bonding network (E16/R32/H58 triad). Conversely, the remaining sites of interaction involve a largely dynamic surface which can accommodate a variety of chemical groups through backbone and side-chain plasticity that have similar affinities resulting from striking enthalpy/entropy compensation.

Given the relatively low specificity of the Src SH2 domain toward short-peptide sequences or small molecule analogs, it may not be possible to identify or design a highly specific inhibitor by only attempting to optimize interactions at the pY + 3 pocket. Indeed, to date, the only Src SH2-targeted inhibitors that are known exploit either the unique cysteine within the pY-binding site or utilize a bisphosphonate pY analog that targets the compound to bone where neighboring osteoclasts

expressing Src kinase at high levels can absorb such compounds.[15–17,63,64]

ACKNOWLEDGMENTS

We thank Dr. Richard Harris (UCL) and Dr. Geoff Kelly (National Institute of Medical Research, Mill Hill) for their assistance with NMR spectroscopy. J.E.L is a Wellcome Trust Senior Research Fellow.

REFERENCES

1. Pawson T, Nash P. Assembly of cell regulatory systems through protein interaction domains. Science 2003;300:445–452.
2. Pawson T. Specificity in signal transduction: from phosphotyrosine-SH2 domain interactions to complex cellular systems. Cell 2004; 116:191–203.
3. Ladbury JE, Arold S. Searching for specificity in SH domains. Chem Biol 2000;7:R3–R8.
4. O'Rourke L, Ladbury JE. Specificity is complex and time consuming: mutual exclusivity in tyrosine kinase-mediated signaling. Acc Chem Res 2003;36:410–416.
5. Songyang Z, Shoelson SE, Chaudhuri M, Gish G, Pawson T, Haser WG, King F, Roberts T, Ratnofsky S, Lechleider RJ, Neel BG, Birge RB, Fajardo JE, Chou MM, Hanafusa H, Schaffhausen B, Cantley LC. SH2 domains recognize specific phosphopeptide sequences. Cell 1993;72: 767–778.
6. Songyang Z, Shoelson SE, Mcglade J, Olivier P, Pawson T, Bustelo XR, Barbacid M, Sabe H, Hanafusa H, Yi T, Ren R, Baltimore D, Ratnofsky S, Feldman RA, Cantley LC. Specific motifs recognized by the SH2 domains of Csk, 3bp2. Fps Fes Grb-2, Hcp Shc Syk, and Vav. Mol Cellular Biol 1994;14:2777–2785.
7. Campbell SJ, Jackson RM. Diversity in the SH2 domain family phosphotyrosyl peptide binding site. Protein Eng 2003;16:217–227.
8. Bradshaw JM, Mitaxov V, Waksman G. Mutational investigation of the specificity determining region of the Src SH2 domain. J Mol Biol 2000;299:521–535.
9. Waksman G, Kominos D, Robertson SC, Pant N, Baltimore D, Birge RB, Cowburn D, Hanafusa H, Mayer BJ, Overduin M, Resh MD, Rios CB, Silverman L, Kuriyan J. Crystal-structure of the phosphotyrosine recognition domain SH2 of V-Src complexed with tyrosine-phosphorylated peptides. Nature 1992;358:646–653.
10. Bradshaw JM, Waksman G. Calorimetric examination of high-affinity Src SH2 domain-tyrosyl phosphopeptide binding: dissection of the phosphopeptide sequence specificity and coupling energetics. Biochemistry 1999;38:5147–5154.
11. Chung E, Henriques D, Renzoni D, Zvelebil M, Bradshaw JM, Waksman G, Robinson CV, Ladbury JE. Mass spectrometric and thermodynamic studies reveal the role of water molecules in complexes formed between SH2 domains and tyrosyl phosphopeptides. Struct Fold Des 1998;6:1141–1151.
12. Lubman OY, Waksman G. Structural and thermodynamic analysis of the peptide binding specificity of the SH2 domain of Src kinase. Biophys J 2002;82:330a.
13. Domchek SM, Auger KR, Chatterjee S, Burke TR, Shoelson SE. Inhibition of SH2 domain phosphoprotein association by a nonhydrolyzable phosphonopeptide. Biochemistry 1992;31:9865–9870.
14. Burke TR, Smyth MS, Otaka A, Nomizu M, Roller PP, Wolf G, Case R, Shoelson SE. Nonhydrolyzable phosphotyrosyl mimetics for the preparation of phosphatase-resistant SH2 domain inhibitors. Biochemistry 1994;33:6490–6494.
15. Violette SM, Shakespeare WC, Bartlett C, Guan W, Smith JA, Rickles RJ, Bohacek RS, Holt DA, Baron R, Sawyer TK. A Src SH2 selective binding compound inhibits osteoclast-mediated resorption. Chem Biol 2000;7:225–235.
16. Shakespeare W, Yang M, Bohacek R, Cerasoli F, Stebbins K, Sundaramoorthi R, Azimioara M, Vu C, Pradeepan S, Metcalf C, Haraldson C, Merry T, Dalgarno D, Narula S, Hatada M, Lu XD, van Schravendijk MR, Adams S, Violette S, Smith J, Guan W, Bartlett C, Herson J, Iuliucci J, Weigele M, Sawyer T. Structure-based design of an osteoclast-selective, nonpeptide Src homology 2 inhibitor with in vivo antiresorptive activity. Proc Natl Acad Sci USA 2000;97:9373–9378.
17. Violette SM, Guan W, Bartlett C, Smith JA, Bardelay C, Antoine E, Rickles RJ, Mandine E, Van Schravendijk MR, Adams SE, Lynch BA, Shakespeare WC, Yang M, Jacobsen VA, Takeuchi CS, Macek KJ, Bohacek RS, Dalgarno DC, Weigele M, Lesuisse D, Sawyer TK, Baron R. Bone-targeted Src SH2 inhibitors block Src cellular activity and osteoclast-mediated resorption. Bone 2001;28:54–64.
18. Bohacek RS, Dalgarno DC, Hatada M, Jacobsen VA, Lynch BA, Macek KJ, Merry T, Metcalf CA, III, Narula SS, Sawyer TK, Shakespeare WC, Violette SM, Weigele M. X-ray structure of citrate bound to Src SH2 leads to a high-affinity, bone-targeted Src SH2 inhibitor. J Med Chem 2001;44:660–663.
19. Taylor JD, Gilbert PJ, Williams MA, Pitt WR, Ladbury JE. Identification of novel fragment compounds targeted against the pY pocket of v-Src SH2 by computational and NMR screening and thermodynamic evaluation. Proteins 2007;67:981–990.
20. Lesuisse D, Lange G, Deprez P, Benard D, Schoot B, Delettre G, Marquette JP, Broto P, Jean-Baptiste V, Bichet P, Sarubbi E, Mandine E. SAR and X-ray. A new approach combining fragment-based screening and rational drug design: application to the discovery of nanomolar inhibitors of Src SH2. J Med Chem 2002;45:2379–2387.
21. Levinson AD, Oppermann H, Levintow L, Varmus HE, Bishop JM. Evidence that the transforming gene of avian sarcoma virus encodes a protein kinase associated with a phosphoprotein. Cell 1978;15: 561–572.
22. Collett MS, Erikson RL. Protein kinase activity associated with the avian sarcoma virus src gene product. Proc Natl Acad Sci USA 1978;75:2021–2024.
23. Takeya T, Hanafusa H. Structure and sequence of the cellular gene homologous to the RSV src gene and the mechanism for generating the transforming virus. Cell 1983;32:881–890.
24. Martin GS. The road to Src. Oncogene 2004;23:7910–7917.
25. Ladbury JE. Protein–protein recognition in phosphotyrosine-mediated intracellular signalling. Proteomics and protein–protein interactions: biology, chemistry, bioinformatics, and drug design. In: Waksman G, editor. New York: Kluwer; ISBN 0–387-24531–6. pp 165–184.
26. Hubbard SR. Src autoinhibition: let us count the ways. Nat Struct Biol 1999;6:711–714.
27. Yang KJ, Shin S, Piao L, Shin E, Li Y, Park KA, Byun HS, Won M, Hong J, Kweon GR, Hur GM, Seok JH, Chun T, Brazil DP, Hemmings BA, Park J. Regulation of 3-phosphoinositide-dependent protein kinase-1 (PDK1) by Src involves tyrosine phosphorylation of PDK1 and Src SH2 domain binding. J Biol Chem 2008;283:1480–1491.
28. Schaller MD, Hildebrand JD, Shannon JD, Fox JW, Vines RR, Parsons JT. Autophosphorylation of the focal adhesion kinase, pp125FAK, directs SH2-dependent binding of pp60src. Mol Cell Biol 1994;14:1680–1688.
29. Nakamoto T, Sakai R, Ozawa K, Yazaki Y, Hirai H. Direct binding of C-terminal region of p130Cas to SH2 and SH3 domains of Src kinase. J Biol Chem 1996;271:8959–8965.
30. Twamley-Stein GM, Pepperkok R, Ansorge W, Courtneidge SA. The Src family tyrosine kinases are required for platelet-derived growth factor-mediated signal transduction in NIH 3T3 cells. Proc Natl Acad Sci USA 1993;90:7696–7700.
31. Frame MC. Src in cancer: deregulation and consequences for cell behaviour. Biochim Biophys Acta 2002;1602:114–130.
32. Verbeek BS, Vroom TM, Adriaansen-Slot SS, Ottenhoff-Kalff AE, Geertzema JG, Hennipman A, Rijksen G. c-Src protein expression is increased in human breast cancer. An immunohistochemical and biochemical analysis. J Pathol 1996;180:383–388.

33. Weber TK, Steele G, Summerhayes IC. Differential pp60c-src activity in well and poorly differentiated human colon carcinomas and cell lines. J Clin Invest 1992;90:815–821.
34. Boyce BF, Yoneda T, Lowe C, Soriano P, Mundy GR. Requirement of pp60c-src expression for osteoclasts to form ruffled borders and resorb bone in mice. J Clin Invest 1992;90:1622–1627.
35. Hall TJ, Schaeublin M, Missbach M. Evidence that c-src is involved in the process of osteoclastic bone resorption. Biochem Biophys Res Commun 1994;199:1237–1244.
36. Yoneda T, Lowe C, Lee CH, Gutierrez G, Niewolna M, Williams PJ, Izbicka E, Uehara Y, Mundy GR. Herbimycin A, a pp60c-src tyrosine kinase inhibitor, inhibits osteoclastic bone resorption in vitro and hypercalcemia in vivo. J Clin Invest 1993;91:2791–2795.
37. Xu RX, Word JM, Davis DG, Rink MJ, Willard DH, Jr, Gampe RT, Jr. Solution structure of the human pp60c-src SH2 domain complexed with a phosphorylated tyrosine pentapeptide. Biochemistry 1995;34:2107–2121.
38. Xu W, Doshi A, Lei M, Eck MJ, Harrison SC. Crystal structures of c-Src reveal features of its autoinhibitory mechanism. Mol Cell 1999;3:629–638.
39. Waksman G, Shoelson SE, Pant N, Cowburn D, Kuriyan J. Binding of a high-affinity phosphotyrosyl peptide to the Src SH2 domain: crystal structures of the complexed and peptide-free forms. Cell 1993;72:779–790.
40. Holland D, Lunney E, Plummer M, Mueller W, McConnell P, Pavlovsky A, Para K, Shahripour A, Humblet C, Sawyer T, Rubin J. Novel pp60Src SH2 domain crystal structures: a 2.0 Å co-crystal structure of a D-amino acid substituted phosphopeptide complex and a 2.1 Å Apo structure displaying self-association. Unpublished report associated with 1BKL entry of PDB; 1997.
41. Cowan-Jacob SW, Fendrich G, Manley PW, Jahnke W, Fabbro D, Liebetanz J, Meyer T. The crystal structure of a c-Src complex in an active conformation suggests possible steps in c-Src activation. Structure 2005;13:861–871.
42. Hobbs CJ, Bit RA, Cansfield AD, Harris B, Hill CH, Hilyard KL, Kilford IR, Kitas E, Kroehn A, Lovell P, Pole D, Rugman P, Sherborne BS, Smith IE, Vesey DR, Walmsley DL, Whittaker D, Williams G, Wilson F, Banner D, Surgenor A, Borkakoti N. Structure-based design of peptidomimetic antagonists of p56(lck) SH2 domain. Bioorg Med Chem Lett 2002;12:1365–1369.
43. Delaglio F, Grzesiek S, Vuister GW, Zhu G, Pfeifer J, Bax A. NMRPIPE—a multidimensional spectral processing system based on UNIX pipes. J Biomol NMR 1995;6:277–293.
44. Kraulis PJ, Domaille PJ, Campbellburk SL, Vanaken T, Laue ED. Solution structure and dynamics of Ras P21.GDP determined by heteronuclear 3-dimensional and 4-dimensional NMR-spectroscopy. Biochemistry 1994;33:3515–3531.
45. Taylor JD, Fawaz RR, Ababou A, Williams MA, Ladbury JE. NMR Assignment of the Apo and peptide-bound SH2 domain from the Rous sarcoma viral protein Src. J Biomol NMR 2005;32:339.
46. Rieping W, Habeck M, Bardiaux B, Bernard A, Malliavin TE, Nilges M. ARIA2: automated NOE assignment and data integration in NMR structure calculation. Bioinformatics 2007;23:381–382.
47. Brunger AT, Adams PD, Clore GM, DeLano WL, Gros P, Grosse-Kunstleve RW, Jiang JS, Kuszewski J, Nilges M, Pannu NS, Read RJ, Rice LM, Simonson T, Warren GL. Crystallography and NMR system: a new software suite for macromolecular structure determination. Acta Crystallogr D 1998;54:905–921.
48. Lipari G, Szabo A. Model-free approach to the interpretation of nuclear magnetic-resonance relaxation in macromolecules. I. Theory and range of validity. J Am Chem Soc 1982;104:4546–4559.
49. Lipari G, Szabo A. Model-free approach to the interpretation of nuclear magnetic-resonance relaxation in macromolecules. II. Analysis of experimental results. J Am Chem Soc 1982;104:4559–4570.
50. Henderson LJ. Concerning the relationship between the strength of acids and their capacity to preserve neutrality. Am J Physiol 1908;21:173–179.
51. DeLano WL. The PyMOL Molecular Graphics System. Palo Alto, CA: DeLano Scientific; 2002.
52. Koradi R, Billeter M, Wuthrich K. MOLMOL: a program for display and analysis of macromolecular structures. J Mol Graph 1996;14:29–32,51–55.
53. Bradshaw JM, Mitaxov V, Waksman G. Investigation of phosphotyrosine recognition by the SH2 domain of the Src kinase. J Mol Biol 1999;293:971–985.
54. Machida K, Mayer BJ. The SH2 domain: versatile signaling module and pharmaceutical target. Biochim Biophys Acta-Proteins Proteom 2005;1747:1–25.
55. Zhang WX, Smithgall TE, Gmeiner WH. Self-association and backbone dynamics of the Hck SH2 domain in the free and phosphopeptide-complexed forms. Biochemistry 1998;37:7119–7126.
56. Kay LE, Muhandiram DR, Farrow NA, Aubin Y, FormanKay JD. Correlation between dynamics and high affinity binding in an SH2 domain interaction. Biochemistry 1996;35:361–368.
57. Finerty PJ, Muhandiram R, Forman-Kay JD. Side-chain dynamics of the SAP SH2 domain correlate with a binding hot spot and a region with conformational plasticity. J Mol Biol 2002;322:605–620.
58. Kristensen SM, Siegal G, Sankar A, Driscoll PC. Backbone dynamics of the C-terminal SH2 domain of the p85 alpha subunit of phosphoinositide 3-kinase: effect of phosphotyrosine-peptide binding and characterization of slow conformational exchange processes. J Mol Biol 2000;299:771–788.
59. Kay LE, Muhandiram DR, Wolf G, Shoelson SE, Forman-Kay JD. Correlation between binding and dynamics at SH2 domain interfaces. Nat Struct Biol 1998;5:156–163.
60. Singer AU, FormanKay JD. pH titration studies of an SH2 domain-phosphopeptide complex: unusual histidine and phosphate pK_a values. Prot Sci 1997;6:1910–1919.
61. Bradshaw JM, Waksman G. Calorimetric investigation of proton linkage by monitoring both the enthalpy and association constant of binding: application to the interaction of the Src SH2 domain with a high-affinity tyrosyl phosphopeptide. Biochemistry 1998;37:15400–15407.
62. Boerner RJ, Consler TG, Gampe RT, Weigl D, Willard DH, Davis DG, Edison AM, Loganzo F, Kassel DB, Xu RX, Patel IR, Robbins JS, Lansing T, Gilmer TM, Luther MA, Knight WB. Catalytic activity of the SH2 domain of human pp60(C-Src). Evidence from NMR, mass-spectrometry site-directed mutagenesis and kinetic-studies for an inherent phosphatase-activity. Biochemistry 1995;34:15351–15358.
63. Alligood KJ, Charifson PS, Crosby R, Consler TG, Feldman PL, Gampe RT, Gilmer TM, Jordan SR, Milstead MW, Mohr C, Peel MR, Rocque W, Rodriguez M, Rusnak DW, Shewchuk LM, Sternbach DD. The formation of a covalent complex between a dipeptide ligand and the src SH2 domain. Bioorg Med Chem Lett 1998;8:1189–1194.
64. Charifson PS, Shewchuk LM, Rocque W, Hummel CW, Jordan SR, Mohr C, Pacofsky GJ, Peel MR, Rodriguez M, Sternbach DD, Consler TG. Peptide ligands of pp60(c-src) SH2 domains: a thermodynamic and structural study. Biochemistry 1997;36:6283–6293.